Available online at www.sciencedirect.com
ScienceDirect
Electrochemistry Communications 9 (2007) 2229–2234
electrochemistry communications
www.elsevier.com/locate/elecom

Composite of Pt–Ru supported SnO_2 nanowires grown on carbon paper for electrocatalytic oxidation of methanol

Madhu Sudan Saha, Ruying Li, Xueliang Sun *

Department of Mechanical and Materials Engineering, The University of Western Ontario, London, Ontario, Canada N6A 5B9

Received 19 May 2007; received in revised form 14 June 2007; accepted 15 June 2007
Available online 30 June 2007

Abstract

Platinum–ruthenium (Pt–Ru) nanoparticles were successfully deposited, for the first time, on the surface of SnO_2 nanowires grown directly on carbon paper (Pt–Ru/SnO_2 NWs/carbon paper) by potentiostatic electrodeposition method. The resultant Pt–Ru/SnO_2 NWs/carbon paper composites were characterized by scanning electron microscopy (SEM), transmission electron microscopy (TEM) and X-ray diffraction (XRD). The electrocatalytic activities of these composite electrodes for methanol oxidation were investigated and higher mass and specific activities in methanol oxidation were exhibited as compared to Pt–Ru catalysts deposited on glassy carbon electrode.

Keywords: SnO_2 nanowires; Pt–Ru nanoparticles; Methanol oxidation reaction; Electrocatalysts; Direct methanol fuel cells; Electrodeposition

1. Introduction

Among the various types of fuel cell, the direct methanol fuel cells (DMFCs) have attracted much attention as green power sources especially for portable applications because of their high energy conversion efficiency, low pollutant emission, low operating temperature, and simplicity of handling and processing of liquid fuel [1]. Electrocatalysts with higher activity for methanol oxidation at room temperature are needed to enhance DMFCs' performance for commercial applications. To date, the most efficient catalyst used for the methanol oxidation in an acidic medium is platinum (Pt) and its alloys such as Pt–Ru [2,3]. The major problems in developing DMFCs with acid media are the slow methanol electro-oxidation reaction kinetics at conventional Pt anode electrocatalysts. The poor kinetics of methanol oxidation at the anode is mostly due to self-poisoning of the surface by reaction intermediates such as CO, which are formed during dehydrogenation of the methanol [4]. Therefore, in order to improve the efficiency of the DMFCs, anode electrocatalysts having a high activity for methanol dehydrogenation and an improved tolerance towards CO poisoning are required [5].

Carbon black (Vulcan XC-72) is widely used as support materials for fuel cell applications [6]. In spite of the high surface area of the carbon black particles, current fuel cell technology still suffers from low Pt utilization, limited mass transport capability, and the limited electrochemical stability of the carbon black-based support in the electrode structure [7]. Therefore, various alternatives of electrocatalyst supports are being searched. Recently, nanostructured carbon materials with graphitic structure, such as carbon nanotubes (CNTs) and carbon fibers were utilized as catalyst supports [8] due to their unique structure and properties such as high surface area, good electronic conductivity, strong mechanical properties and chemical stability [9,10]. Several research groups have demonstrated the advantages of using CNTs and carbon fibers as supports to better disperse Pt and Pt–Ru alloys for methanol oxidation reactions [11–14]. Compared with carbon black,

* Corresponding author. Tel.: +1 519 661 2111x87759; fax: +1 519 661 3020.
E-mail address: xsun@eng.uwo.ca (X. Sun).

1388-2481/$ - see front matter © 2007 Elsevier B.V. All rights reserved.
doi:10.1016/j.elecom.2007.06.032

a higher durability of carbon nanotube-based electrodes has been revealed [15]. Particularly, the growth of CNTs directly on carbon paper (fuel cell baking) as catalyst support has shown unique advantage to improve Pt utilization because of their three-dimensional (3-D) structure [16–18].

More recently, various metal oxides have been explored as catalyst support [19–22]. Among of them, SnO_2 particles as Pt support have been used for PEMFCs and DMFCs, and have revealed high catalytic activities toward methanol oxidation [23]. One of the advantages of SnO_2 support is that it has strong chemical interactions with metallic components [24]. While these studies utilized its form of the particles, our interests are to directly grow SnO_2 nanowires (NWs) on fuel cell backings as catalyst support for fuel cells in order to build 3-D electrode structure. In our recent report, we have synthesized the SnO_2 NWs directly on the carbon fibers of carbon paper by a thermal evaporation method with subsequent deposition of Pt nanoparticles to improve the Pt utilization [25]. In this communication, we report the electrodeposition of Pt–Ru nanoparticles on the surface of the SnO_2 NWs directly grown on carbon fiber of carbon paper. The electrocatalytic activities of these novel composites for the methanol oxidation reaction are reported here.

2. Experimental

2.1. Synthesis of SnO_2 NWs on carbon paper

The synthesis of SnO_2 NWs on the fibers of a carbon paper (E-TEK Division, PEMEAS Fuel Cell Technologies, Somerset, NJ) was carried out by a thermal evaporation method. In a typical experiment, an alumina boat loaded with 2 g of Sn powder (325 mesh, 99.8%) was placed in the middle of a quartz tube (1.8 cm inner diameter and 75 cm length) and inserted into a horizontal tube furnace. A piece of carbon paper (1 cm × 1 cm) was placed beside the metal powder. The reaction chamber was heated to 800 °C from room temperature with an argon (Ar) flow rate of 200 sccm (standard cubic centimeters per minute). Subsequently, the furnace was kept at 800 °C for 2 h and then cooled to room temperature. After the reaction, a dense white wool-like product was observed on the surface of the carbon substrate. During the heating, the Sn vapor generated from the Sn power combines with oxygen (O_2), which comes from the residue O_2 in the reaction chamber or from the Ar gas, to form SnO_2 NWs.

2.2. Electrodeposition of Pt–Ru nanoparticles

The deposition of Pt–Ru nanoparticles and electrochemical measurements were performed using an Autolab potentiostat/galvanostat (Model, PGSTAT-30, Ecochemie, Brinkman Instruments) in a three-electrode, two-compartment configuration cell. A Pt wire served as the counter electrode and a saturated calomel electrode (SCE) were used as the reference electrode. All potentials in this report are quoted against SCE. Purified Ar (99.9998%) and O_2 (<99.5%) gases were purchased from Praxair Canada Inc.

Before Pt–Ru nanoparticles deposition, the SnO_2 NWs grown directly on carbon paper (SnO_2 NWs/carbon paper) was pretreated chemically in 5.0 M HNO_3 aqueous solution for 6 h. To further increase the electrochemical activity of the surface of the SnO_2 NWs in water solution [26], the SnO_2 NWs/carbon paper electrode was then cycled in the range of −0.15 to +1.3 V vs SCE at a scan rate of 50 mV/s in 0.5 M H_2SO_4 aqueous solution for 20 cycles. Pt–Ru nanoparticles supported on the SnO_2 NWs/carbon paper were prepared by potentiostatic method at applied potential of −0.25 V vs SCE [27]. Pt–Ru nanoparticles were electrodeposited from 0.5 M H_2SO_4 aqueous solution containing 0.2 mM $H_2PtCl_6 \cdot H_2O$ (Aldrich) and 0.2 mM $RuCl_3 \cdot xH_2O$ (Aldrich) solutions. Pt–Ru nanoparticles supported SnO_2 NWs/carbon paper composite was denoted as Pt–Ru/SnO_2 NWs/carbon paper. For comparison, Pt–Ru particles were also deposited on the glassy carbon (GC, diameter 3 mm) electrode at the same deposition condition, denoted as Pt–Ru/GC. After the deposition procedure, the electrodes were removed from the deposition solution and thoroughly rinsed with deionized water. For the measurement of hydrogen electrosorption curves, the potential was cycled between −0.25 and +0.9 V at 50 mV/s to obtain the voltammograms of hydrogen adsorption in Ar-purged 0.5 M H_2SO_4 aqueous solution. For CO stripping voltammetry, pure CO (99.5%) was purged closed to the working electrode for at least 1 h with the electrode polarized at 0.2 V vs SCE in a fume hood. The electrode was then purged with pure Ar for 1 h under potential control followed by voltammetric stripping. For cyclic voltammetry (CV) of methanol oxidation, the electrolyte solution was 2 M CH_3OH in 1 M H_2SO_4 aqueous solution. All experiments were carried out at room temperature (25 °C). The Pt loading was determined by inductively coupled plasma-optical emission spectroscopy (ICP-OES).

2.3. Morphological and structural characterization

Scanning electron microscope (SEM) (Hitachi S-2600 N) and transmission electron microscopy (TEM) (Philips CM10) were employed to examine the morphologies of SnO_2 NWs/carbon paper before and after electrodeposition of Pt–Ru nanoparticles. X-ray diffraction (XRD) analysis was carried out with an X-ray diffractometer (Rigaku-MiniFlex) using Cu K α radiation at 30 kV.

3. Results and discussion

Fig. 1 shows typical SEM and TEM images of the SnO_2 NWs grown on carbon fibers of carbon paper by thermal evaporation method. The carbon fibers of about 5–10 μm in diameter cross each other (inset in Fig. 1a). From Fig. 1a, it can be seen that high-density SnO_2 NWs fully cover the fibers of the carbon paper. The length of SnO_2

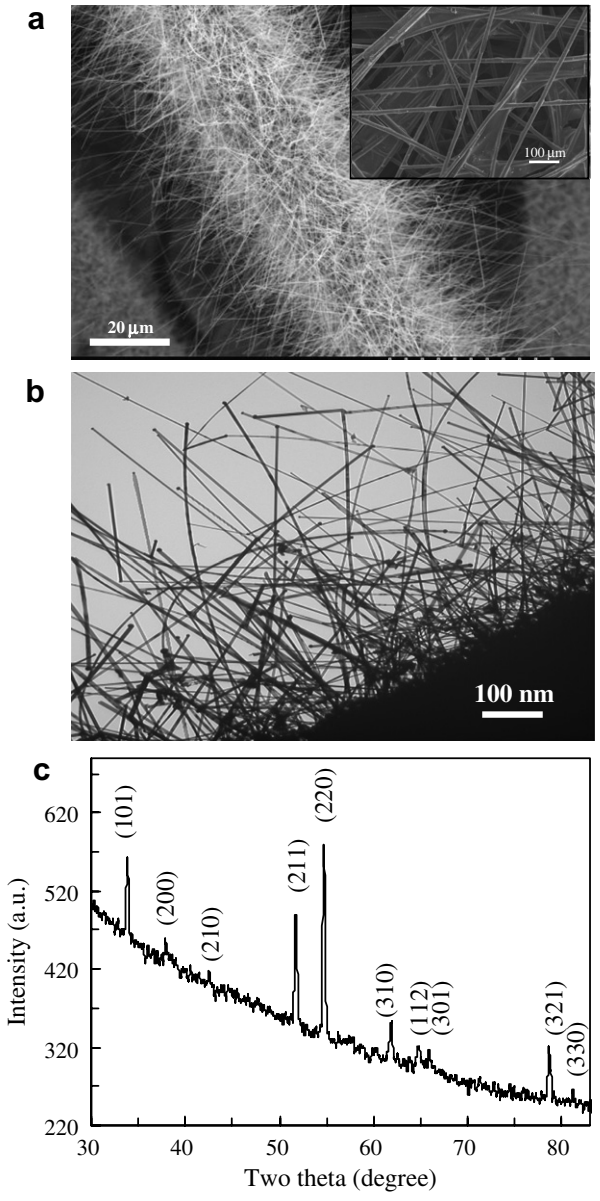

Fig. 1. SnO_2 NWs grown on carbon fibers of carbon paper by thermal evaporation method: (a) SEM image showing high coverage of SnO_2 NWs on fibers of carbon paper (inset: fibers of bare carbon paper); (b) TEM image of SnO_2 NWs/carbon paper indicating morphologies of the nanowires; and (c) XRD pattern of as-prepared SnO_2 NWs/carbon paper composite.

NWs is about 15–20 μm. The typical TEM image shown in Fig. 1b reveals that the nanowires are straight with diameters of 30–100 nm. XRD pattern of as-prepared SnO_2 NWs/carbon paper shows the crystalline structure of SnO_2 NWs (Fig. 1c). The diffraction peaks at around 37.9°, 51.7°, 54.0°, 62.3° and 66.1° are assigned to SnO_2 (101), (211), (220), (310) and (301), respectively, indicating that the nanowires are composed of SnO_2.

Fig. 2a shows TEM images of Pt–Ru nanoparticles deposited on SnO_2 NWs grown on carbon paper by potentiostatic electrodeposition method. A lot of Pt–Ru nanoparticles with sizes ranging from 25 to 35 nm were

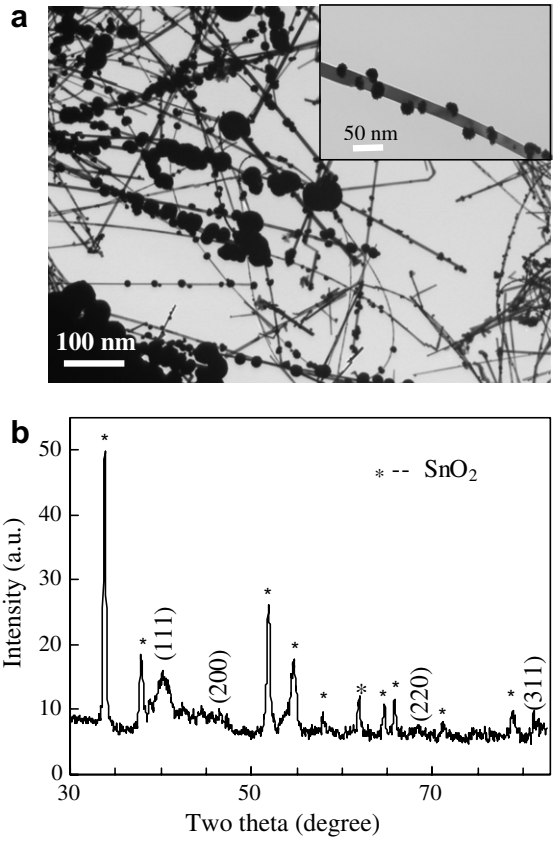

Fig. 2. (a) TEM image of Pt–Ru nanoparticles deposited on SnO_2 NWs/carbon paper by potentiostatic method (inset: Pt–Ru nanoparticles deposited onto a single SnO_2 NW) and (b) XRD pattern of Pt–Ru nanoparticles supported on SnO_2 NWs/carbon paper.

dispersed uniformly onto the surface of SnO_2 NWs. Furthermore, some relatively large metal particles on the SnO_2 NWs/carbon paper were observed. On the contrary, Pt–Ru nanoparticles deposited on the CNTs surface by potentiostatic electrodeposition had a larger particle size of 150 nm in diameter [28]. XRD analysis of the Pt–Ru/SnO_2 NWs/carbon paper composite in Fig. 2b reveals the presence of peaks at around 40.4°, 46.9°, 68.1° and 83.06° [29]. These peaks can be assigned to (111), (200), (220) and (311) of Pt–Ru alloys, confirming the crystallinity of the Pt–Ru nanoparticles. This indicates that Pt–Ru/SnO_2 NWs/carbon paper composite has been successfully prepared.

Fig. 3a shows CVs of the Pt–Ru/SnO_2 NWs/carbon paper composite in Ar-saturated 0.5 M H_2SO_4 in order to examine whether Pt–Ru particles deposited on the SnO_2 NWs support. For comparison, control experiments under the identical experimental conditions were performed for the Pt–Ru particles electrodeposition on GC electrode and the corresponding results are also presented in Fig. 3a. It can be seen that all of the characteristics of Pt–Ru alloy have been displayed [30]. The Pt–Ru/SnO_2 NWs/carbon paper composite electrode has the higher current response for the hydrogen adsorption and deposition than that of the Pt–Ru/GC. Fig. 3b shows adsorbed CO

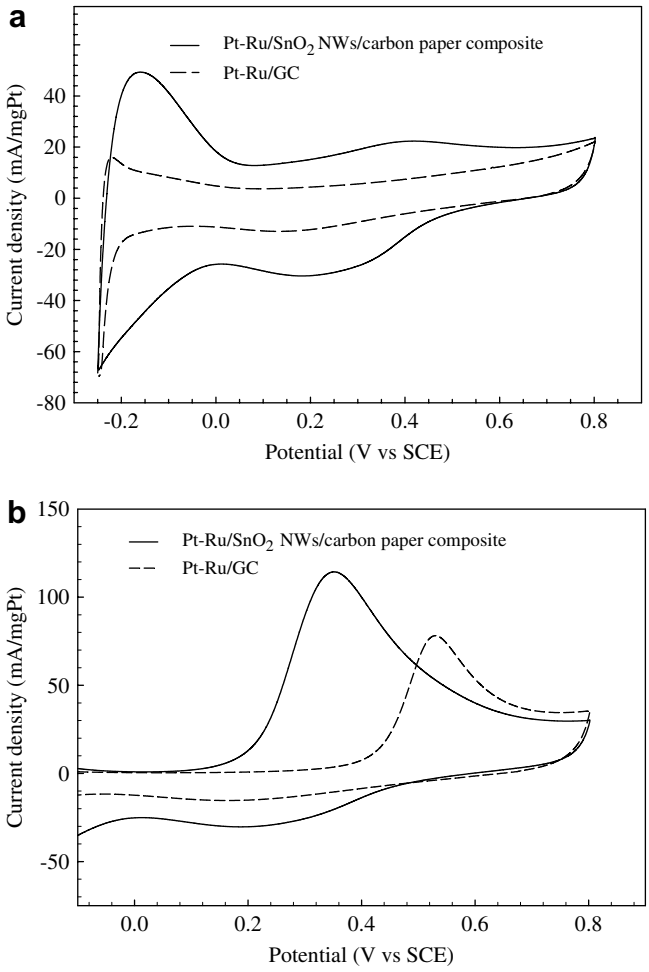

Fig. 3. Cyclic voltammograms of Pt–Ru nanoparticles electrodeposited on SnO_2 NWs/carbon paper and GC electrodes (a) in the absence and (b) presence of CO in 0.5 M H_2SO_4 aqueous solution at room temperature. Potential scan rate: 50 mV/s. The CO was absorbed at 0.2 V for 1 h, subsequently, the solution CO was removed by Ar bubbling for 1 h while maintaining the potential at 0.2 V vs SCE.

(CO_{ads}) stripping voltammograms for the Pt–Ru/SnO_2 NWs/carbon paper composite and Pt–Ru/GC electrodes in 0.5 M H_2SO_4 solution at 50 mV/s. CO was purged while holding the potential at 0.20 V vs SCE for 1 h at 25 °C. The oxidation peak of CO_{ads} is more negative for the Pt–Ru/SnO_2 NWs/carbon paper composite than the Pt–Ru/GC electrode, indicating the CO_{ads} oxidation becomes energetically more favorable at Pt–Ru/SnO_2 NWs/carbon paper composite electrode. The roughness factor (r_f) and the real Pt surface (A_{EL}, m^2/g_{Pt}) from CO_{ads} stripping were measured using the following equations [31]:

$$r_f(cm^2/cm^2) = Q_{CO_{ads}}/420\ \mu C\ cm^{-2} \quad (1)$$

$$A_{EL}(m^2/g_{Pt}) = r_f/Pt \quad \text{loading}. \quad (2)$$

The electrochemically active surface area of the Pt–Ru/SnO_2 NWs/carbon paper composite and Pt–Ru/GC electrode were also estimated from the integrated charge in the hydrogen adsorption and desorption region of the CVs. The calculated values of roughness factors (cm^2/cm^2) as well as roughness factors normalized on the basis of Pt loading are listed in Table 1. Comparison of roughness factors (cm^2/cm^2) and mass specific surface areas (m^2/g) obtained from CO_{ads} and H_{upd} indicates remarkable agreement. In the case of Pt–Ru/SnO_2 NWs/carbon paper composite, the electrochemical surface areas are significantly higher as compared to the Pt–Ru/GC electrode (approximately 43%) (Table 1). This difference is attributed to the unique 3-D structure of the SnO_2 NWs-based electrode and smaller size of Pt nanoparticles on the SnO_2 NWs.

Table 1
Real (active) surface areas of Pt–Ru/SnO_2 NWs/carbon paper and Pt–Ru/GC electrodes obtained from CO_{ads} stripping voltammetry and H_{ads}/H_{des} regions of the voltammograms

Electrode	Pt loading[a] ($\mu g/cm^2$)	Q_H (mC/cm^2)	S_{EL}[b] (cm^2/cm^2)	A_{EL}[c] (m^2/g_{Pt})
Pt–Ru/SnO_2 NWs	45.56	10.6	25.3 (23.8)	55.4 (52.2)
Pt–Ru/GC	47.73	5.7	13.6 (10.4)	28.5 (21.8)

[a] Measured by inductively coupled plasma-optical emission spectroscopy.
[b] S_{EL}: real surface area obtained electrochemically, the values in bracket is obtained from the average of hydrogen adsorption/desorption peaks.
[c] A_{EL}: real surface area obtained electrochemically per gram of Pt catalyst, the values in bracket is obtained from the average of hydrogen adsorption/desorption peaks.

Fig. 4 shows a comparison of catalytic activities for Pt–Ru nanoparticles supported SnO_2 NWs/carbon paper and GC electrodes in 2 M CH_3OH/1 M H_2SO_4 at a scan rate of 50 mV/s. While bare SnO_2 NWs/carbon paper without Pt–Ru nanoparticles was used as electrode, there was no current response for methanol oxidation, indicating that SnO_2 NWs are not active for methanol oxidation (not shown). After the Pt–Ru deposition, typical features of methanol oxidation were observed in Fig. 4, which is

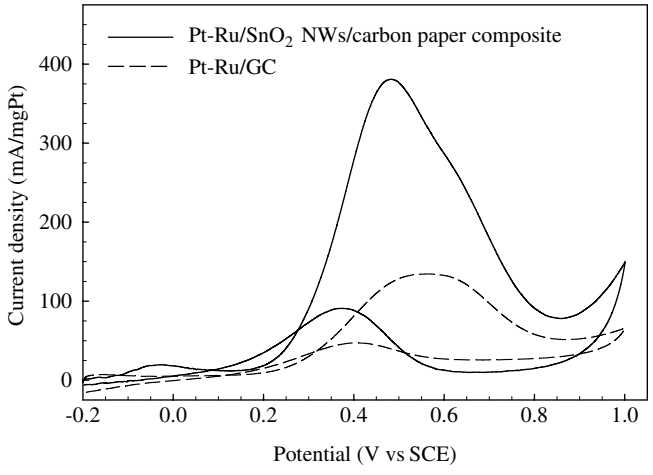

Fig. 4. Cyclic voltammograms of Pt–Ru nanoparticles electrodeposited on SnO_2 NWs/carbon paper and GC electrodes in Ar-saturated 1 M H_2SO_4 + 2 M MeOH aqueous solution. Potential scan rate: 50 mV/s.

Table 2
Electrochemical characteristics of methanol oxidation on Pt–Ru/SnO_2 NWs/carbon paper and Pt–Ru/GC electrodes

Electrode	Onset potential (V)	Forward peak current density (mA/cm^2)	Forward peak potential (V)	Mass activity (mA/mg Pt)	Specific activity (mA/cm^2 Pt)	i_f/i_b ratio
Pt–Ru/SnO_2 NWs	0.173	17.5	0.478	383.8	0.692	4.11
Pt–Ru/GC	0.188	6.2	0.559	128.7	0.452	3.34

All electrochemical data were taken from the CVs shown in Fig. 4.

in good agreement with literature [32]. It is clearly evident that the Pt–Ru/SnO_2 NWs/carbon paper composite has considerably higher methanol oxidation current (3.2 mA/cm^2) than that of the Pt–Ru/GC electrode (1.3 mA/cm^2) at a potential of 0.3 V. Moreover, the Pt–Ru nanoparticles supported on the SnO_2 NWs/carbon paper electrode have a lower onset potential (ca. 0.173 V) than the one on GC electrode (ca. 0.188 V), indicating better electrocatalytic activity of Pt–Ru/SnO_2 NWs/carbon paper electrode. All electrochemical characteristic data of the tests are summarized in Table 2.

There are two ways to explain the activities of Pt based electrocatalysts. One is mass activity (MA) associated with the current per amount of catalyst, and the other is specific activity (SA) related to surface area of Pt. The MA has significant implications for fuel cells, because the cost of electrode largely depends on the total catalysts, while the SA provides catalytic information of Pt atoms in the surface. The various parameters including MA (peak current density of methanol oxidation obtained from CV per unit of Pt loading mass) [33], SA (peak current normalized with Pt surface area) and the ratio of the forward oxidation current peak (i_f) to the reverse current peak (i_b) are also shown in Table 2. According to the MA data listed in Table 2, the Pt–Ru/SnO_2 NWs/carbon paper composite showed better electrocatalytic activities for methanol oxidation than the Pt–Ru/GC electrode. The Pt–Ru supported on SnO_2 NWs/carbon carbon showed a higher methanol oxidation current, and the MA is 383.8 mA/mg Pt, which is 66% higher than Pt–Ru supported on GC electrode (128.7 mA/mg Pt), suggesting a higher catalyst utilization for methanol oxidation reaction. Further, it has also been shown that the SA of Pt–Ru/SnO_2 NWs/carbon paper composite (0.692 mA/cm^2 Pt) is slightly higher than the Pt–Ru/GC electrode (0.452 mA/cm^2 Pt). This indicates that the Pt–Ru/SnO_2 NWs/carbon paper composite have a good improvement in methanol oxidation activity.

The i_f/i_b ratio is an index of the catalyst tolerance to CO species [34]. From Table 2, the i_f/i_b ratio of SnO_2 NWs-based electrode is higher than that of the GC electrode, indicating more effective removal of the CO species on the catalyst surface of SnO_2 NWs-based electrode. The higher electrocatalytic activities for methanol oxidation at Pt–Ru/SnO_2 NWs/carbon paper composite may be attributed to the unique 3-D structure [16,35] and electronic properties of SnO_2 NWs [36]. We have revealed that the growth of SnO_2 NWs directly on carbon paper can form 3-D electrode structure with a larger surface area [25]. It was also believed that catalyst support interactions can modify the electronic nature of metal catalyst particles [24], resulting in enhanced catalytic activity. It was reported that Pt catalysts supported on SnO_2 film or particles show higher catalytic activities toward methanol oxidation [23,37]. Further, the CO tolerance of Pt was improved by the addition of oxides such as SnO_2 and MoO_2 [38,39]. The role of these oxides was proposed to relax the strong CO adsorption on Pt, which originates in the modification of the electronic band structure of Pt and the interaction between Pt and metal oxides [38,39].

The stability of the SnO_2 NWs/carbon paper composite was also investigated by immersing the composite electrode in 0.1 M H_2SO_4 solution over a period of 1500 h at 50 °C. After the stability test, SEM and TEM observations reveal that high-density SnO_2 NWs are still on the surface of carbon fibers and the diameter of SnO_2 NWs is no change, suggesting strong adhesion between SnO_2 NWs and the carbon paper as well as high stability of SnO_2 NWs.

4. Conclusions

The 3-D composite electrodes consisting of Pt–Ru/SnO_2 NWs/carbon paper have been successfully synthesized by growing SnO_2 NWs on carbon paper and subsequently deposition of Pt–Ru nanoparticles on the NWs. The CV measurements showed that the Pt–Ru/SnO_2 NWs/carbon paper composite electrodes have considerably higher methanol oxidation mass activity and specific activity as well as better CO tolerance for methanol oxidation reaction than one supported on the GC electrode. These results imply that the supporting materials and electrode structure are critical factors on the catalytic activities. This may provide a new route to take advantage of large surface-to-volume ratio metal oxide NWs-based catalyst supports for DMFC applications.

Acknowledgements

This research was supported by Natural Sciences and Engineering Research Council of Canada (NSERC), Canada Foundation for Innovation (CFI), Ontario Research Fund (ORF), Ontario Early Researcher Award (ERA) and the University of Western Ontario, Academic Development Fund (ADF) and the Start-up Fund.

References

[1] M. Winter, R.J. Brodd, Chem. Rev. 104 (2004) 4245.
[2] T. Matsumoto, T. Komatsu, K. Arai, T. Yamazaki, M. Kijima, H. Shimizu, Y. Takasawa, J. Nakamura, Chem. Commun. (2004) 840.

[3] T.J. Schmidt, U.A. Paulus, H.A. Gasteiger, R.J. Behm, J. Electroanal. Chem. 508 (2001) 41.
[4] J.-M. Leiger, J. Appl. Electrochem. 31 (2001) 767.
[5] H.A. Gasteiger, N. Markovic, P.N. Ross, E.J. Cairns, J. Electrochem. Soc. 141 (1994) 1795.
[6] C. Bock, C. Paquet, M. Couillard, G.A. Botton, B.R. MacDougall, J. Am. Chem. Soc. 126 (2004) 8028.
[7] H.A. Gasteiger, S.S. Kocha, B. Sompalli, F.T. Wagner, Appl. Catal. B: Environ. 56 (2005) 9.
[8] H. Liu, C. Songa, L. Zhang, J. Zhang, H. Wang, D.P. Wilkinson, J. Power Sources 155 (2006) 95.
[9] R.M. Baum, Chem. Eng. News 75 (1997) 39.
[10] R.H. Baughman, A.A. Zakhidov, W.A. Heer, Science 297 (2002) 787.
[11] W. Li, C. Liang, W. Zhou, J. Qiu, Z. Zhou, G. Sun, Q. Xin, J. Phys. Chem. B 107 (2003) 6292.
[12] N. Rajalakshmi, H. Ryu, M.M. Shaijumon, S. Ramaprabhu, J. Power Sources 140 (2005) 250.
[13] G. Girishkumar, K. Vinodgopal, P.V. Kamat, J. Phys. Chem. B 108 (2004) 19960.
[14] E.S. Steigerwalt, G.A. Deluga, C.M. Lukehart, J. Phys. Chem. B 106 (2002) 760.
[15] Y. Shao, G. Yin, Y. Gao, P. Shi, J. Electrochem. Soc. 153 (2006) A1093.
[16] X. Sun, R. Li, D. Villers, J.P. Dodelet, S. Desilets, Chem. Phys. Lett. 379 (2003) 99.
[17] C. Wang, M. Waje, X. Wang, J.M. Tang, R.C. Haddon, Y. Yan, Nano. Lett. 4 (2004) 345.
[18] D. Villers, S.H. Sun, A.M. Serventi, J.P. Dodelet, J. Phys. Chem. B 110 (2006) 25916.
[19] O.S. Alexeev, S.Y. Chin, M.H. Engelhard, L. Ortiz-Soto, M.D. Amiridis, J. Phys. Chem. B 109 (2005) 23430.
[20] H. Chhina, S. Campbell, O. Kesler, J. Power Sources 161 (2006) 893.
[21] R. Ganesan, J.S. Lee, J. Power Sources 157 (2006) 217.
[22] Z. Tang, G. Lu, J. Power Sources 162 (2006) 1067.
[23] L. Jiang, G. Sun, Z. Zhou, S. Sun, Q. Wang, S. Yan, H. Li, J. Tian, J. Guo, B. Zhou, Q. Xin, J. Phys. Chem. B 109 (2005) 8774.
[24] S.J. Tauster, S.C. Fung, R.T.K. Baker, J.A. Horsley, Science (Washington, DC, US) 211 (1981) 1121.
[25] M.S. Saha, R. Li, M. Cai, X. Sun, Electrochem. Solid-State Lett. 10 (2007) B130.
[26] P. Eraymundo, A.D. Cazorla, S.A. Linares, S. Delpeux, E. Frackowiak, K. Szostak, F. Beguin, Carbon 40 (2002) 1597.
[27] C.-H. Lee, C.-W. Lee, D.-I. Kim, S.-E. Bae, Int. J. Hydrogen Energy 27 (2002) 445.
[28] M.-C. Tsai, T.-K. Yeh, Z.-Y. Juang, C.-H. Tsai, Carbon 45 (2007) 383.
[29] K.-T. Jeng, C.-C. Chien, N.-Y. Hsub, S.-C. Yen, S.-D. Chiou, S.-H. Lin, W.-M. Huanga, J. Power Sources 160 (2006) 97.
[30] H.A. Gasteiger, N. Markov, P.N.J. Ross, E.J. Cairns, J. Phys. Chem. B 97 (1993) 12020.
[31] C. Bock, M.-A. Blakey, B.R. MacDougall, Electrochim. Acta 50 (2005) 2401.
[32] W.X. Chen, J.Y. Lee, Z. Liu, Chem. Commun. (2002) 2588.
[33] F. Gloaguen, J.-M. Leger, C. Lamy, J. Appl. Electrochem. 27 (1997) 1052.
[34] Y. Mu, H. Liang, J. Hu, L. Jiang, L. Wan, J. Phys. Chem. B 109 (2005) 22212.
[35] X. Wang, M. Waje, Y. Yan, Electrochem. Solid-State Lett. 8 (2005) A42.
[36] J.-S. Lee, S.-K. Sim, B. Min, K. Cho, S.W. Kim, S. Kim, J. Cryst. Growth 267 (2004) 145.
[37] A.L. Santos, D. Profeti, P. Olivi, Electrochim. Acta 50 (2005) 2615.
[38] T. Matsui, K. Fujiwara, T. Okanishi, R. Kikuchi, T. Takeguchi, K. Eguchi, J. Power Sources 155 (2006) 152.
[39] T. Ioroi, N. Fujiwara, Z. Siroma, K. Yasuda, Y. Miyazaki, Electrochem. Commun. 4 (2002) 442.